Temperature enhances exocytosis efficiency at the mouse inner hair cell ribbon synapse

Régis Nouvian

InnerEarLab, Department of Otolaryngology, Center for Molecular Physiology of the Brain, Bernstein Center for Computational Neuroscience, Göttingen University Medical School, Robert-Koch-Strasse 40, 37075 Göttingen, Germany

Hearing relies on fast and sustained neurotransmitter release from inner hair cells (IHCs) onto the afferent auditory nerve fibres. The temperature dependence of Ca^{2+} current and transmitter release at the IHCs ribbon synapse has not been investigated thus far. To assess the influence of temperature on calcium-triggered exocytosis, patch-clamp recordings of voltage-gated L-type Ca^{2+} influx and exocytic membrane capacitance changes were performed at room (25°C) and physiological (35–37°C) temperatures. An increase in temperature within this range increased the L-type Ca^{2+} current amplitude of IHCs ($Q_{10} = 1.3$) and accelerates the activation kinetics. Fast exocytosis, probed by 20 ms depolarization, was enhanced at physiological temperature with a Q_{10} of 2.1. The amplitude of fast release was elevated disproportionately to the increase in Ca^{2+} influx. In contrast, the rate of sustained exocytosis (exocytic rate between 20 and 100 ms of depolarization) did not show a significant increase at physiological temperature. Altogether, these data indicate that the efficiency of fast exocytosis is higher at physiological temperature than at room temperature and suggest that the number of readily releasable vesicles available at the active zone is higher at physiological temperature.

(Resubmitted 27 June 2007; accepted after revision 21 August 2007; first published online 23 August 2007)
Corresponding author R. Nouvian: Department of Otolaryngology, Göttingen University Medical School, Robert-Koch-Strasse 40, 37075 Göttingen, Germany. Email: nouvian@med.uni-goettingen.de

Synaptic coding at the inner hair cell (IHC) ribbon synapse in the cochlea is a fundamental step in hearing. To achieve temporally precise synaptic transmission, IHC active zones make use of a large readily releasable pool of synaptic vesicles (RRP, e.g. Moser & Beutner, 2000; Spassova *et al.* 2001; Griesinger *et al.* 2005; Khimich *et al.* 2005; Rutherford & Roberts, 2006; recent reviews in Moser *et al.* 2006; Nouvian *et al.* 2006). The RRP is thought to represent the docked and primed vesicles of active zone (Nouvian *et al.* 2006), which upon exocytosis are rapidly replaced by new releasable vesicles. This rapid re-supply mediates, at least in part, the sustained exocytic component observed by presynaptic capacitance measurements (e.g. Moser & Beutner, 2000; Eisen *et al.* 2004; Schnee *et al.* 2005), optical imaging (Griesinger *et al.* 2005) and recordings of postsynaptic excitatory currents (Keen & Hudspeth, 2006). To date, with some exceptions (see Fig. 1 of Moser & Beutner; 2000; Johnson *et al.* 2005), all presently available biophysical studies of hair cell transmitter release have been carried out at room temperature. This, in addition to other details (such as the whole-cell configuration) of *in vitro* experiments, limits meaningful comparisons to *in vivo* findings, such as peristimulus time histograms of auditory nerve fibre spiking. Moreover, the temperature dependence of hair cell presynaptic function has not been directly studied.

Neurosecretion has been shown to be highly temperature sensitive in various preparations (Bittner & Holz; 1992; Thomas *et al.* 1993; Renstrom *et al.* 1996; Hardingham & Larkman, 1998; Dinkelacker *et al.* 2000; Pyott & Rosenmund, 2002; Volgushev *et al.* 2004; Kushmerick *et al.* 2006). While typically describing boosting effects of temperature on transmitter release, these studies arrived at different conclusions about the affected synaptic properties. Some concluded that the increased temperature resulted in an enhanced rate of vesicle supply to the readily releasable pool (Bittner & Holz; 1992; Thomas *et al.* 1993; Renstrom *et al.* 1996; Dinkelacker *et al.* 2000; Pyott & Rosenmund, 2002; Kushmerick *et al.* 2006), while others described an increased release probability (Hardingham & Larkman, 1998; Volgushev *et al.* 2004). Moreover, the kinetics of endocytotic membrane retrieval following transmitter release were described as being highly temperature sensitive (Fernandez-Alfonso & Ryan, 2004; Micheva & Smith, 2005).

The aim of this study was to investigate how temperature affects transmitter release in the IHC, which

 DOI: 10.1113/jphysiol.2007.139675

serves as an important model for studying presynaptic Ca^{2+} signalling and stimulus–secretion coupling due to its excellent experimental accessibility (review in Moser *et al.* 2006). The influence of temperature on calcium current properties was first described by using whole-cell patch-clamp recordings. However, to directly compare presynaptic function at room and body temperature in individual cells, recordings were performed under perforated patch-clamp configuration, which enables long-lasting recordings by preserving the cytosolic integrity of the cell. Altogether, this study provides evidence that both Ca^{2+} influx and exocytosis are temperature-dependent in IHCs.

Methods

Patch-clamp recordings of Ca^{2+} currents and membrane capacitance (C_m)

The animals were maintained according to the animal welfare guidelines of the University of Göttingen and the State of Lower Saxony. After cervical dislocation of C57Bl6/N mice (postnatal day 13 (P13) to 16 (P16)), IHCs of the apical coil of freshly dissected organs of Corti were patch clamped at their basolateral face at room (25°C) and physiological temperature (35–37°C) in perforated-patch and whole-cell configuration as previously described (Brandt *et al.* 2003). The pipette solution for perforated-patch recordings contained (mM): 130 Cs-gluconate, 10 tetraethylammonium-Cl (TEA-Cl), 10 Hepes buffer, 1 $MgCl_2$ and 10 4-aminopyridine (4-AP) as well as 250 μg ml^{-1} amphotericin B; for standard whole-cell experiments, pipette solution contained: 130 Cs-gluconate, 10 TEA-Cl, 10 Hepes buffer, 1 $MgCl_2$, 10 4-AP, 2 Mg-ATP, 0.3 Na-GTP and 0.1 ethyleneglycol-bis(β-aminoethylether)-*N*,*N*,*N*′,*N*′-tetraacetic acid (EGTA). The extracellular solution contained (mM): 105 NaCl, 35 TEA-Cl, 2.8 KCl, 1 $MgCl_2$, 10 Hepes, 2 $CaCl_2$ and 10 D-glucose. For whole-cell experiments, 1 mM CsCl was added in order to efficiently block KCNQ conductance (Wong *et al.* 2004). Solutions were adjusted to pH 7.2 and had osmolarities between 290 and 310 mosmol l^{-1}. Solution changes were achieved by slow bath exchange. All chemicals were obtained from Sigma (St Louis, MO, USA), with the exception of CsOH (Aldrich, Milwaukee, WI, USA) and amphotericin B (Calbiochem, La Jolla, CA, USA).

The Ca^{2+} current was, to some extent, still contaminated by other remaining currents despite the choice of ionic conditions (probably a mixture of KCNQ4, BK and delayed rectifier potassium currents, transduction current and leak currents). In whole cell recordings, Ca^{2+} current was further isolated using *P*/*n* protocols (usually 15 leak pulses with amplitudes of 20% of the original pulse from a holding potential of −117 mV) or by subtracting a linear function extrapolated from the current–voltage relationship at a hyperpolarized voltage range (between −97 mV and −77 mV). In some experiments, an increase in the resting current was observed upon switching to physiological temperature, which was reversible upon returning to room temperature; however, the change of the average extrapolated reversal potential of the resting membrane current was negligible upon switching to physiological temperature (−59.8 ± 1.1 mV to −59.7 ± 0.8 mV at room and physiological temperature, respectively, $n = 9$). In perforated-patch clamp, Ca^{2+} current integrals were calculated from the total depolarization-evoked inward current, including Ca^{2+} tail currents after *P*/6 leak subtraction (i.e. from the start of the depolarization step to 1.5 ms after the end of the depolarization step). Cells that displayed a membrane current exceeding −60 pA at −87 mV and at room temperature were discarded from the analysis. No series resistance (R_s) compensation was applied, but recordings with $R_s > 30$ MΩ and $R_s > 7$ MΩ for perforated and whole-cell patch-clamp experiments, respectively, were discarded from the analysis. In perforated-patch experiments, current was low-pass filtered at 4 kHz and sampled at 10 kHz for exocytic ΔC_m and at 40 kHz for Ca^{2+} current recordings. In whole-cell experiments, currents were low-pass filtered at 10 kHz and sampled at 50 kHz for Ca^{2+} current recordings. All voltages were corrected for liquid junction potentials calculated between pipette and bath (for room and physiological temperature, respectively: 16.9 mV and 17.5 mV in perforated-patch; 16.7 mV and 17.5 mV in whole-cell recordings).

Capacitance measurements

C_m was measured using the Lindau–Neher technique (Lindau & Neher, 1988), implemented in the software-lockin module of Pulse (HEKA Elektronik, Lambrecht, Germany) combined with compensation of pipette and resting cell capacitances by the EPC-9 (HEKA Elektronik) compensation circuitries. A 1 kHz, 70 mV peak-to-peak sinusoid was applied about the holding potential of −87 mV. ΔC_m was estimated as the difference of the mean C_m over 400 ms after the end of the depolarization (the initial 250 ms was skipped) and the mean prepulse capacitance (400 ms). Mean ΔC_m and Ca^{2+} current estimates present grand averages calculated from the mean estimates of individual IHCs. Data analysis was performed using Igor Pro software (WaveMetrics, Lake Oswego, OR, USA). Means are expressed ± S.E.M. and compared by Student's unpaired (whole-cell patch-clamp) and paired (perforated patch-clamp) *t* test.

Temperature control

Temperature was adjusted by flow-heating and heating of the objective lens with a temperature/heater controller

(type TC-344B, Warner, Hamden, CT, USA). Temperature was measured by a miniature thermistor close to the organ of Corti. Influence of temperature on calcium current properties was first investigated on two different populations of IHCs (at room and physiological temperature); however, to allow direct comparison of secretory responses between room and physiological temperature, the effects of successive changes in temperature (25°C, 35–37°C and 25°C) in individual cells were observed. The transitions took ∼5–10 min (35–37°C) and 10–20 min (25°C). The temperature sensitivity Q_{10} (i.e. the coefficient by which rates or factors of interest, R_1 and R_2, are increased by a change of 10°C), was calculated using the equation: $Q_{10} = (R_2/R_1)^{(10/\Delta T)}$, where R_1 and R_2 were measured at room and physiological temperature, respectively.

Results

Larger Ca^{2+} currents at physiological temperature

The temperature sensitivity of the voltage-gated L-type Ca^{2+} channels (mostly $Ca_V1.3$ channels; Platzer *et al.* 2000; Brandt *et al.* 2003; Brandt *et al.* 2005) that trigger release of synaptic vesicles at the IHC active zones was first investigated. In order to resolve submillisecond activation kinetics of I_{Ca}, these experiments were conducted in whole-cell configuration. Figure 1*A* displays

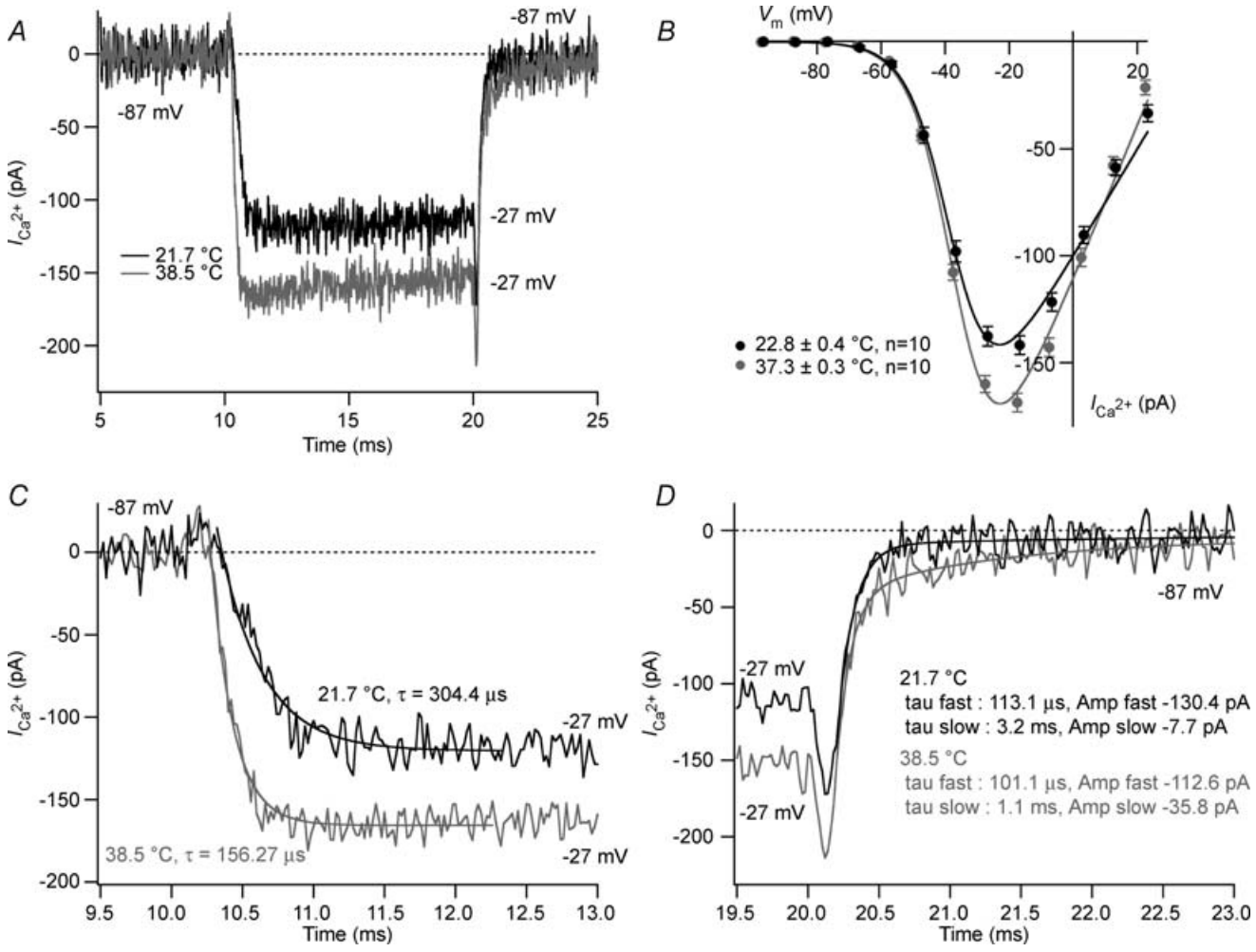

Figure 1. Temperature effects on voltage-gated Ca^{2+} currents IHCs
A, I_{Ca} recorded from two IHCs at room and physiological temperature (P15). Currents were recorded by applying a 10 ms voltage step from the holding potential (i.e. −87 mV) to −27 mV. Capacitive transients were subtracted using a *P*/15 protocol. For room and physiological temperature, respectively: R_s = 5.5 MΩ and 5.8 MΩ; resting membrane capacitance = 9.7 pF and 9.7 pF; resting current at holding potential (−87 mV) = −1.7 pA and −12.2 pA. *B*, steady-state *I–V* at the different temperatures: steady-state amplitude was measured as the average over 4 ms starting 4 ms after the beginning of the 10 ms test pulse ($n = 10$). IV curves were fitted by a first order Boltzmann equation times the driving force (see text). *C*, calcium currents of *A* on expanded time scale. Activation kinetics time constant derived from the single exponential fit over 2 ms after the residual capacitive transients. *D*, tail current of *A* on expanded time scale. Tails current were best approximated by a double exponential fit (see text).

Table 1. Biophysical properties of the IHCs recorded in whole-cell experiments under room and physiological temperature

	22.8 ± 0.4°C	37.3 ± 0.3°C
C_m (pF)	9.7 ± 0.2	9.0 ± 0.2
I_{ss} (pA)	−12.8 ± 3.1	−8.3 ± 1.2
R_s (MΩ)	6.0 ± 0.1	5.4 ± 0.2
V_h (mV)	−37.2 ± 0.6	−35.8 ± 0.4
k (mV)	6.4 ± 0.1	6.5 ± 0.1

I_{ss} is the steady-state current recorded at the holding potential (−87 mV). V_h and k are from fits using a first order Boltzmann equation times the driving force. $n = 10$, values are means ± S.E.M.

I_{Ca} of representative 2-week-old IHCs elicited by a 10 ms depolarization to −27 mV at 21.7 and 38.5°C. The steady-state I_{Ca} of IHCs, measured at −17 mV, at 37°C (168.6 ± 4.3 pA, $n = 10$) was significantly larger ($P < 0.0001$) than that of IHCs at 23°C (141.8 ± 4.3 pA, $n = 10$) as shown in Fig. 1*B*. The corresponding Q_{10} was approximately 1.13, which is lower than the Q_{10} obtained when I_{Ca} was probed in perforated patch-clamp experiments (Q_{10} of 1.3, see Physiological temperature increases release efficiency of fast exocytosis). This discrepancy could arise from the heterogeneity of samples taken in the whole-cell recordings (comparison of one population of IHCs at room temperature to another group of IHCs at body temperature), in contrast to the perforated patch-clamp experiments, which probed temperature effects in individual IHCs that experience successive temperature changes.

An example of the influence of temperature on the activation kinetics of I_{Ca} is shown in detail in Fig. 1*C*. The time constants of I_{Ca} were obtained by fitting the traces with the following equation:

$$I(t) = A_1 + A_2 \exp(-t/\tau),$$

where I is the current amplitude at time t, A_1 and A_2 are constants and τ is the activation time constant. At 23°C, I_{Ca} activates rapidly, with an activation time constant that decreased with depolarization (from 420.2 ± 32.4 μs measured at −47 mV to 213.2 ± 10.7 μs measured at −7 mV, $n = 10$). At 37°C, analysis of the activation time constant after P/15 correction revealed an acceleration of the activation kinetics (from 247.4 ± 27.1 μs measured at −47 mV to 108.6 ± 8.8 μs measured at −7 mV, $n = 10$; $P < 0.0001$).

Inward tail currents occurring upon repolarization to −87 mV are shown on an expanded time scale (Fig. 1*E*). The tail currents decay with a time course that was best approximated with the following double exponential fit:

$$I(t) = A_1 + A_2 \exp(-t/\tau_1) + A_3 \exp(-t/\tau_2),$$

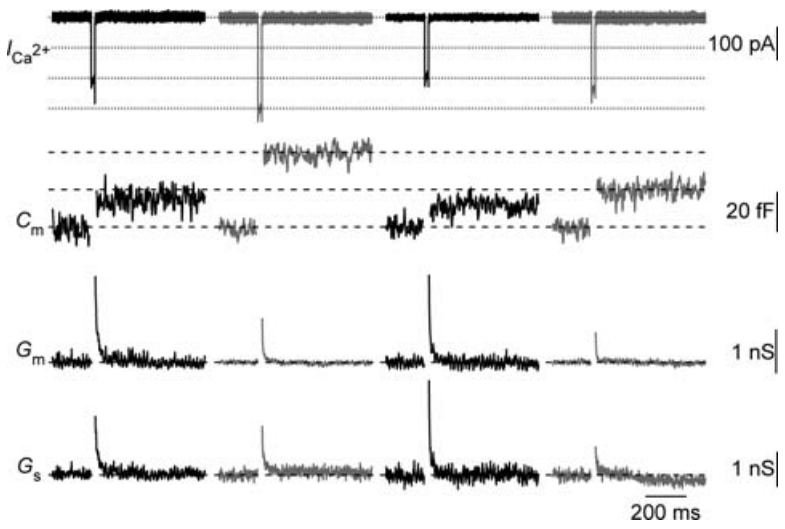

Figure 2. Increased fast exocytosis at body temperature
Representative Ca^{2+} current (I_{Ca}), membrane capacitance (C_m) low-pass filtered at 100 Hz, membrane conductance (G_m) and series conductance (G_s) traces (from top to bottom) elicited by depolarizations from holding potential (−87 mV) to −17 mV measured at different temperatures. The data were obtained from one IHC in which two changes in temperature were performed. Early transient changes in membrane conductance (G_m) or series conductance (G_s) were observed but these changes did not correlate temporally or in amplitude with the C_m response. For the first round of temperature changes, at room and physiological temperature, respectively: $R_s = 17.9$ MΩ and 11.8 MΩ; resting membrane capacitance = 9.2 pF and 9.3 pF; resting current at holding potential (−87 mV) = −31.7 pA and −82.2 pA. For the second round of temperature changes, at room and physiological temperature, respectively: $R_s = 14.4$ MΩ and 11.9 MΩ; resting membrane capacitance = 9.3 pF and 9.8 pF; resting current at holding potential (−87 mV) = −35.1 pA and −74.4 pA.

where I is the current amplitude at time t, A_1, A_2, A_3 are constants and τ_1 and τ_2 are the deactivation time constants. Whereas the fast component is on the order of a hundred microseconds ($101.9 \pm 5.1\ \mu s$), the slow component is on the order of milliseconds (2.8 ± 0.9 ms) at 23°C ($n = 10$). At 37°C, tail current analysis revealed larger slow component amplitude (-18.5 ± 3.4 pA *versus* -33.5 ± 2.1 pA from -27 mV to -87 mV at 23 and 37°C, respectively, $n = 10$, $P < 0.005$). However, the nature of the latter component was not investigated in more detail in this study.

Current voltage curves obtained by step depolarizations were fitted according to:

$$I = G_{max}(V - V_{rev})/1 + \exp\{(V_h - V/k\})$$

where I is the current amplitude, V is the membrane potential, V_{rev} is the extrapolated reversal potential, G_{max} is the maximal conductance of the cell, V_h is the voltage for half-maximal activation and k is the slope factor of the Boltzmann function. In contrast to the changes in amplitudes and activation kinetics, I_{Ca} activation curve did not show any appreciable difference in V_h ($P > 0.1$; Table 1) and in voltage sensitivity k ($P > 0.5$; Table 1).

Increased fast and sustained exocytosis at physiological temperature

Exocytic membrane capacitance increments (ΔC_m) were recorded to assess the influence of temperature on neurotransmitter release. Exocytic secretion was probed with perforated patch-clamp, which allowed for the monitoring of capacitance jumps in response to depolarizations of different durations while successively changing temperature from 25 to 35–37°C and back.

Figure 2 shows C_m traces (second panel) of a P15 IHC in response to 20 ms of depolarization to the peak Ca^{2+} current potential under succesive changes in temperature (from 25°C to 35°C, followed by the return to 25°C and after then warming up to 35°C). The change in temperature to 35°C augmented fast exocytosis (probed with the exocytic response to 20 ms depolarization), which is mediated by the readily releasable pool (RRP; Moser & Beutner, 2000; Khimich *et al.* 2005). Smaller exocytic responses were observed after the return to room temperature than before warming. However, the I_{Ca} amplitude recorded after the return to room temperature was nearly identical to that observed at the beginning of the experiments under room temperature (Fig. 3). Altogether, this suggests a secretory run-down of the IHCs synapse during the time course of the experiment. Among nine cells recorded to assess the impact of temperature on exocytosis, five cells have been successfully recorded with a complete second warming cycle, as illustrated in Fig. 2. On average, smaller exocytic responses were observed after the second increase in temperature (18.7 ± 4.8 fF probed by 20 ms depolarizations, $n = 5$) in comparison to the responses measured after the initial warming (29.7 ± 4.9 fF, probed by 20 ms depolarizations, $n = 5$). Ca^{2+} current influx, however, did not show major differences between the second (4.3 ± 0.5 pC probed by 20 ms depolarizations, $n = 5$) and the first increase in temperature (4.6 ± 0.4 pC probed by 20 ms depolarizations, $n = 5$). This result is in line with a run-down of the secretion at the IHC synapse.

Figure 3 (top panel) compares average exocytic capacitance increments (ΔC_m) obtained with depolarizations of different durations (cumulative exocytosis) between 25 and 35°C, and followed by a re-cooling to 25°C in a total of nine experiments. The increase in temperature significantly enhanced fast

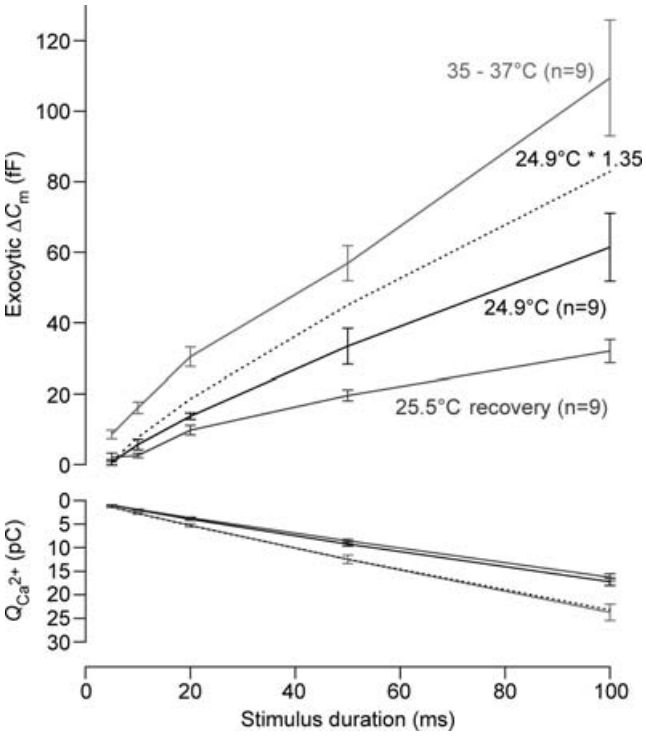

Figure 3. Readily releasable pool exocytosis is affected by elevated temperature
Exocytic ΔC_m (upper panel) and the corresponding Ca^{2+} current integrals (Q_{Ca}, lower panel) are represented *versus* the duration of depolarization (to the potential eliciting the maximal Ca^{2+} current) for room and physiological temperature. The data were obtained from cells that experienced a cycle from room (black) to physiological (grey) and back to room (light grey) temperature. Dotted lines represent (lower panel) the mean Ca^{2+} current integrals at room temperature scaled by a factor of 1.35 to match the physiological temperature data and (upper panel) the cumulative exocytosis at room temperature scaled by the same factor. For room, physiological and back to room temperature, respectively: $R_s = 23.2 \pm 1.5$ MΩ, 15.8 ± 1.6 MΩ and 15.4 ± 1.5 MΩ, resting membrane capacitance = 8.7 ± 0.4 pF, 9.3 ± 0.3 pF and 9.5 ± 0.3 pF, resting current at holding potential (-87 mV) = -41.4 ± 3.4 pA, -77.4 ± 7.9 pA and -43.7 ± 4.5 pA.

exocytosis. Fast release (probed by 20 ms depolarizations) amounted to 13.7 ± 0.9 fF and 30.4 ± 2.7 fF at 25 and 35°C, respectively ($P < 0.001$). On average, temperature enhanced RRP exocytosis with a Q_{10} of 2.1. However, the biggest difference between exocytosis at 25 and 35°C was observed for the shortest stimulus duration (5 ms). Larger ΔC_m responses to 100 ms depolarization pulse were observed at physiological temperature (61.3 ± 9.6 fF *versus* 109.3 ± 16.4 fF at 25 and 35°C, respectively, $P < 0.05$). However, the rate of sustained exocytosis (approximated by linear fitting of cumulative exocytosis between 20 and 100 ms) was not significantly different between room and body temperature (slope: 595 ± 115.4 fF s^{-1} *versus* 987 ± 206.3 fF s^{-1} at 25 and 35°C, respectively; $P = 0.097$). Probably, the high variability in the capacitance in response to the longer depolarization (50 and 100 ms) meant that the measured increase with temperature did not achieve statistical significance.

Physiological temperature increases release efficiency of fast exocytosis

At physiological temperature, calcium influx increases with temperature with a Q_{10} of 1.3 (I_{Ca}: -193.5 ± 11 pA *versus* -259.8 ± 15.6 pA following a depolarization step from -87 mV to -17 mV at 25 and 35°C, respectively, $P < 0.001$). Assuming a Ca^{2+} nanodomain control of exocytosis, the increased release may be taken to reflect recruitment of more active Ca^{2+} channel release site units (Brandt *et al.* 2005). However, linear scaling of cumulative exocytosis with the increase in Ca^{2+} current integrals (factor 1.35, Fig. 3, bottom panel) could not entirely explain the temperature-induced gain of exocytosis (dashed line) indicating an increased exocytic efficiency (i.e. more exocytosis for a given amount of Ca^{2+} influx).

This notion became more obvious when plotting ΔC_m *versus* the corresponding Ca^{2+} current integrals (Fig. 4). At 35°C, more exocytosis was observed per unit of incoming Ca^{2+} ions for the short depolarizations. The ratio of ΔC_m over the Ca^{2+} current integral, Q_{Ca}, for responses to 20 ms amounted to 3.46 ± 0.17 fF pC^{-1} and to 5.85 ± 0.42 fF pC^{-1} at 25 and 35°C, respectively ($P < 0.005$, $n = 9$, Fig. 4*C*). However, in response to 100 ms step depolarization, the release efficiency showed no significant difference between room and physiological temperature (3.53 ± 0.44 fF pC^{-1} *versus* 4.9 ± 0.96 fF pC^{-1} at 25 and 35°C, respectively, $n = 9$, $P > 0.1$). These results argue that temperature has an effect on exocytosis downstream of calcium entry during short depolarizations.

Discussion

This study demonstrates that temperature enhances IHC presynaptic function. RRP exocytosis was increased at physiological temperature with no significant change in the rate of sustained release. The enhancement in fast exocytosis probably involves an increase of exocytosis

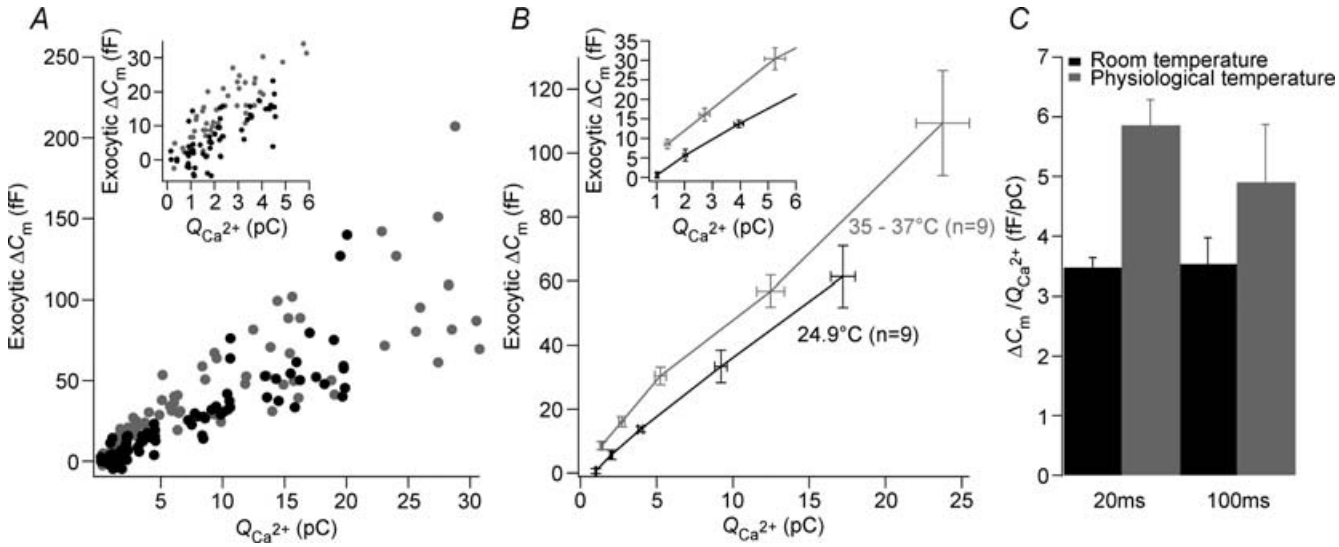

Figure 4. Physiological temperature increase release efficiency
A, relationship of exocytic ΔC_m to their corresponding Ca^{2+} current integrals (Q_{Ca}) to compare the efficiency of exocytosis at room and body temperature. Inset: expanded time scale of *A*. *B*, binned ΔC_m *versus* the corresponding Q_{Ca} according to the stimulus time duration (i.e. 5, 10, 20, 50 and 100 ms). Inset: expanded time scale of *B*. *C*, efficiency of release measured as the ratio $\Delta C_m/Q_{Ca}$, for 20 ms and 100 ms step depolarization to -17 mV from the holding potential of -87 mV, at room and body temperature ($n = 9$).

efficiency. This study implies that experimental results related to the RRP and acquired at room temperature should be scaled up if they are to be related to *in vivo* findings.

Mechanisms underlying the temperature effects on hair cell exocytosis

Physiological temperature enhances Ca^{2+} influx through $Ca_V1.3$ channels into IHCs with an acceleration of the current's activation kinetics. This can be due to an increased open probability and/or conductance of the Ca^{2+} channel at higher temperature (Lux & Brown, 1984; Acerbo & Nobile, 1994). Despite the lack of change in V_h and in voltage sensitivity of the activation curve is in line with an unchanged open probability, the specific effect of temperature on the single Ca^{2+} channel in IHCs remains to be tested in future single channel or fluctuation analysis experiments.

Previous work has suggest that transmitter release at IHC active zones is governed by Ca^{2+} nanodomains (Brandt *et al.* 2005). In the case of an open probability increase upon physiological temperature (Lux & Brown, 1984), the opening of additional Ca^{2+} channels would cause the release of their nearby vesicles resulting in a linear increase of exocytosis with that of the whole-cell Ca^{2+} current. This mechanism is likely to contribute to the observed increase in fast exocytosis but cannot entirely explain it. Indeed, a scaled version of the exocytosis under room temperature using the same factor required to match the Ca^{2+} influx failed to overlap the exocytosis at physiological temperature (Fig. 3).

An increase of single channel current could, by causing a higher $[Ca^{2+}]$ at the vesicle's release site, result in faster exocytosis kinetics and explain at least part of the effect. With the extracellular $[Ca^{2+}]$ at 2 mM, the calcium-triggered exocytic responses were out of the range of the supralinear part of the exocytosis–Ca^{2+} influx relationship (Brandt *et al.* 2005; Johnson *et al.* 2005), i.e. in the steep intrinsic Ca^{2+} dependence in the low micromolar range. Thus, a further $[Ca^{2+}]$ increase does not cause a major change in exocytosis as the $[Ca^{2+}]$ at the release sites has already driven exocytosis to the maximum rate (Brandt *et al.* 2005; Johnson *et al.* 2005). Thus, a potential increase of single Ca^{2+} channel current cannot entirely explain the disproportionate increase of exocytosis.

Therefore, the data obtained in this study suggest that temperature raises the efficiency of fast exocytosis. Potential mechanisms include: (i) Ca^{2+} channel control of more than one nearby vesicle (e.g. by higher abundance of readily releasable vesicles) and (ii) faster kinetics of exocytosis (e.g. due to intrinsic temperature dependence). At present, the mechanism(s) that might be responsible for the observed effects remains unclear.

The increase in release efficiency for fast exocytosis is in line with the demonstration of an accelerated vesicle supply at physiological temperature in many other neurosecretory preparations (Dinkelacker *et al.* 2000; Kushmerick *et al.* 2006). However, the lack of change *per se* in the rate of sustained component is unexpected since it has been proposed that this component may also reflect the vesicle supply to the synapse (Schnee *et al.* 2005; Griesinger *et al.* 2005). An alternative explanation might be that the high scatter of responses for the 100 ms depolarization step observed in these experiments did not reveal a significant change and therefore prevents any definitive conclusion. Further work should be directed at finding out whether more vesicles are available for release at physiological temperature, and whether exocytosis occurs more rapidly.

References

Acerbo P & Nobile M (1994). Temperature dependence of multiple high voltage activated Ca^{2+} channels in chick sensory neurones. *Eur Biophys J* **23**, 189–195.

Bittner MA & Holz RW (1992). A temperature-sensitive step in exocytosis. *J Biol Chem* **267**, 16226–16229.

Brandt A, Khimich D & Moser T (2005). Few $Ca_V1.3$ channels regulate the exocytosis of a synaptic vesicle at the hair cell ribbon synapse. *J Neurosci* **25**, 11577–11585.

Brandt A, Striessnig J & Moser T (2003). $Ca_V1.3$ channels are essential for development and presynaptic activity of cochlear inner hair cells. *J Neurosci* **23**, 10832–10840.

Dinkelacker V, Voets T, Neher E & Moser T (2000). The readily releasable pool of vesicles in chromaffin cells is replenished in a temperature-dependent manner and transiently overfills at 37°C. *J Neurosci* **20**, 8377–8383.

Eisen MD, Spassova M & Parsons TD (2004). Large releasable pool of synaptic vesicles in chick cochlear hair cells. *J Neurophysiol* **91**, 2422–2428.

Fernandez-Alfonso T & Ryan TA (2004). The kinetics of synaptic vesicle pool depletion at CNS synaptic terminals. *Neuron* **41**, 943–953.

Griesinger CB, Richards CD & Ashmore JF (2005). Fast vesicle replenishment allows indefatigable signalling at the first auditory synapse. *Nature* **435**, 212–215.

Hardingham NR & Larkman AU (1998). The reliability of excitatory synaptic transmission in slices of rat visual cortex in vitro is temperature dependent. *J Physiol* **507**, 249–256.

Johnson SL, Marcotti W & Kros CJ (2005). Increase in efficiency and reduction in Ca^{2+} dependence of exocytosis during development of mouse inner hair cells. *J Physiol* **563**, 177–191.

Keen EC & Hudspeth AJ (2006). Transfer characteristics of the hair cell's afferent synapse. *Proc Natl Acad Sci U S A* **103**, 5537–5542.

Khimich D, Nouvian R, Pujol R, Tom Dieck S, Egner A, Gundelfinger ED & Moser T (2005). Hair cell synaptic ribbons are essential for synchronous auditory signalling. *Nature* **434**, 889–894.

Kushmerick C, Renden R & von Gersdorff H (2006). Physiological temperatures reduce the rate of vesicle pool depletion and short-term depression via an acceleration of vesicle recruitment. *J Neurosci* **26**, 1366–1377.

Lindau M & Neher E (1988). Patch-clamp techniques for time-resolved capacitance measurements in single cells. *Pflugers Arch* **411**, 137–146.

Lux HD & Brown AM (1984). Patch and whole cell calcium currents recorded simultaneously in snail neurons. *J Gen Physiol* **83**, 727–750.

Micheva KD & Smith SJ (2005). Strong effects of subphysiological temperature on the function and plasticity of mammalian presynaptic terminals. *J Neurosci* **25**, 7481–7488.

Moser T & Beutner D (2000). Kinetics of exocytosis and endocytosis at the cochlear inner hair cell afferent synapse of the mouse. *Proc Natl Acad Sci U S A* **97**, 883–888.

Moser T, Brandt A & Lysakowski A (2006). Hair cell ribbon synapses. *Cell Tissue Res* **326**, 347–359.

Nouvian R, Beutner D, Parsons TD & Moser T (2006). Structure and function of the hair cell ribbon synapse. *J Membr Biol* **209**, 153–165.

Platzer J, Engel J, Schrott-Fischer A, Stephan K, Bova S, Chen H, Zheng H & Striessnig J (2000). Congenital deafness and sinoatrial node dysfunction in mice lacking class D L-type Ca^{2+} channels. *Cell* **102**, 89–97.

Pyott SJ & Rosenmund C (2002). The effects of temperature on vesicular supply and release in autaptic cultures of rat and mouse hippocampal neurons. *J Physiol* **539**, 523–535.

Renstrom E, Eliasson L, Bokvist K & Rorsman P (1996). Cooling inhibits exocytosis in single mouse pancreatic B-cells by suppression of granule mobilization. *J Physiol* **494**, 41–52.

Rutherford MA & Roberts WM (2006). Frequency selectivity of synaptic exocytosis in frog saccular hair cells. *Proc Natl Acad Sci U S A* **103**, 2898–2903.

Schnee ME, Lawton DM, Furness DN, Benke TA & Ricci AJ (2005). Auditory hair cell-afferent fiber synapses are specialized to operate at their best frequencies. *Neuron* **47**, 243–254.

Spassova M, Eisen MD, Saunders JC & Parsons TD (2001). Chick cochlear hair cell exocytosis mediated by dihydropyridine-sensitive calcium channels. *J Physiol* **535**, 689–696.

Thomas P, Wong JG, Lee AK & Almers W (1993). A low affinity Ca^{2+} receptor controls the final steps in peptide secretion from pituitary melanotrophs. *Neuron* **11**, 93–104.

Volgushev M, Kudryashov I, Chistiakova M, Mukovski M, Niesmann J & Eysel UT (2004). Probability of transmitter release at neocortical synapses at different temperatures. *J Neurophysiol* **92**, 212–220.

Wong WH, Hurley KM & Eatock RA (2004). Differences between the negatively activating potassium conductances of mammalian cochlear and vestibular hair cells. *JARO* **5**, 270–284.

Acknowledgements

I would like to thank T. Moser for his generous support, helpful comments thoughout this project and help with the first version of the manuscript. I also thank H. Taschenberger, A. Neef, A. Meyer and A. Woehler for comments on manuscript and members of the Innerearlab for discussions and suggestions. I would like also to thank the reviewers for their constructive comments. This work was supported by grants of the DFG (SFB406 and CMPB), the European Commission (through the integrated project EuroHear), the Human Frontiers Science Program (HFSP) and the federal government (through the Bernstein Center for Computational Neuroscience, Goettingen) to T. Moser.